A Control Scheme for Utilizing Energy Storage of the Modular Multilevel Converter for Power Oscillation Damping

Abel A. Taffese, Elisabetta Tedeschi
Dept. of Electric Power Engineering
Norwegian University of Science and Technology
Trondheim, Norway
abel.taffese@ntnu.no, elisabetta.tedeschi@ntnu.no

Erik de Jong
Dept. of Electrical Engineering
Technische Universiteit Eindhoven
Eindhoven, The Netherlands
e.c.w.de.jong@tue.nl

***Abstract*—This paper presents a control scheme that utilizes energy storage of the Modular Multilevel Converter (MMC) for Power Oscillation Damping (POD) service. Such a service is used to enhance grid stability by providing damping power in the electromechanical (0.2-2Hz) dynamics range. The scheme uses compensated modulation with average energy control. The aforementioned service comes at the cost of additional energy storage requirement for the MMC. A worst case estimate of this additional capacity, together with potential options to obtain it, is also addressed in this paper. The scheme is validated by simulation studies on a four terminal HVDC test grid.**

***Index Terms*—Power Oscillation Damping, HVDC, Energy Storage, MMC, Modulation, Arm Capacitor, POD**

I. Introduction

Power Oscillation Damping (POD) is one of the ancillary services that can be provided by a voltage sourced converter in a power system. It is a service that improves damping of electromechanical oscillations (typically $0.2-2\ Hz$) in an ac grid by injecting a damping power. VSC-HVDC converter can achieve POD by modulating either active or reactive powers [1], [2]. It was found in [2] that active power modulation gives more robust performance regarding ac voltage variations. However, a side effect of using active power is that the oscillation is exported to the dc side since active power is balanced instantaneously. Ref. [3] addressed this issue by coordinating the POD service between two terminals in such a way that their contributions cancel on the dc side. A better alternative solution is to prevent the oscillation from entering the dc side by using solutions that involve energy storage. The challenge with such solutions is that energy storage technology is relatively expensive and not well-developed for HVDC applications. Fortunately, the Modular Multilevel Converter (MMC), which is the most widely accepted VSC topology, has energy storage capability distributed in its Sub-Modules (SM). This paper proposes a control scheme that will make energy storage of the MMC available for POD. Existing work on POD using MMC[4] focuses on the design of the POD controller and not on the utilization of MMC energy storage. The proposed scheme is based on a closed loop control of the average arm energy of the MMC using compensated modulation as proposed in [5]. It requires an increase in the energy storage capacity such that the POD service can be provided without affecting normal operation. Sizing considerations for the of additional storage are also addressed in this paper. The remainder of this paper is organized as follows. Section II deals with the modeling approach, followed by the control structure in Section IV. Then, the proposed controller is described in Section V. The extra energy storage requirement is treated in Section VI. Simulation results are presented in Section VII. Finally, conclusion is presented in Section VIII.

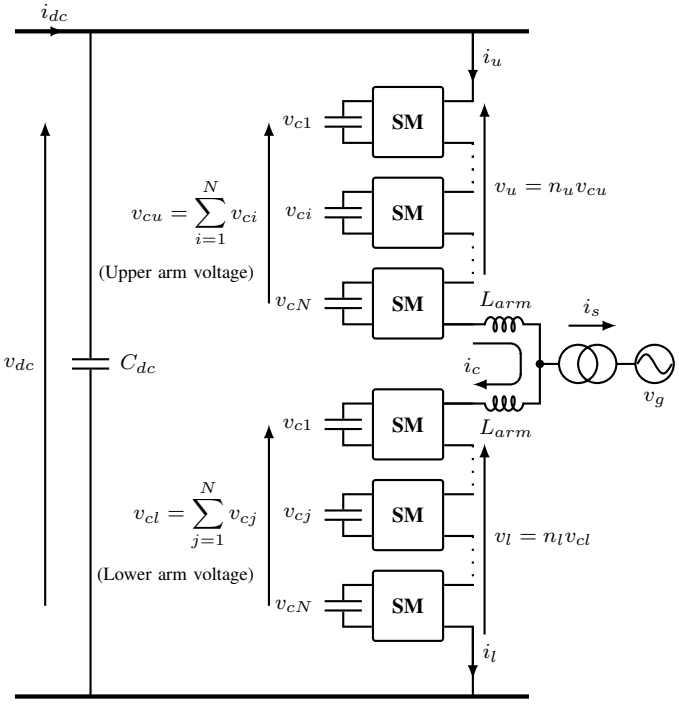

Fig. 1. Per-phase circuit of the MMC.

II. Modeling

This section presents a simplified average model of the MMC. The most important assumptions made in the development of the model are: 1) compensated modulation [5] is used, 2) average energies of upper and lower arms are balanced, and 3) effect of ripples in the average energy can be neglected. First, the concept of compensated modulation will be discussed followed by the dynamic equations describing the MMC.

A. Compensated Modulation

Modulation, in this context, refers to the way the insertion indexes, n_u and n_l, are calculated given the respective inserted voltage references v_u^* and v_l^* (1).

$$v_u^* = \frac{1}{2}\left(v_{dc}^* - v_s^* - 2v_c^*\right) \quad v_l^* = \frac{1}{2}\left(v_{dc}^* + v_s^* - 2v_c^*\right) \tag{1}$$

where v_{dc}^* is the dc link voltage reference, v_s^* is the ac voltage reference, and v_c^* is common mode voltage reference. Direct modulation is the simplest modulation techniques where it is assumed that the arm voltage is ripple-free and equal to the dc link. Thus, the reference voltages are divided by v_{dc} as shown in (2).

$$n_u = \frac{v_u^*}{v_{dc}} \quad and \quad n_l = \frac{v_l^*}{v_{dc}} \tag{2}$$

The corresponding inserted voltages are given by (3).

$$v_u = v_u^* \frac{v_{cu}}{v_{dc}} \quad and \quad v_l = v_l^* \frac{v_{cl}}{v_{dc}} \tag{3}$$

where v_{cu} and v_{cl} are the upper and lower arm voltages, respectively. Since the arm voltages contain dominant first and second harmonic ripples, the inserted voltages will also contain harmonic components resulting in circulating currents. In order to avoid this, the references are divided by the respective arm voltages which cancel out from the inserted voltage as shown in (4). This is the concept behind compensated modulation [5]. The main implication is that the harmonic content in the inserted voltages comes only from the references. This means that undesired circulating current can be avoided without the need for an additional controller.

$$n_u = \frac{v_u^*}{v_{cu}} \implies v_u = v_u^* \frac{v_{cu}}{v_{cu}} = v_u^* \tag{4}$$

The arm voltages are needed to implement compensated modulation. It was discussed [6] that the use of measured arm voltages is not effective because of measurement distortion and the loss of open sloop stability of the arm voltage. The open-loop approach, which uses estimated arm voltages, has been shown to have better stability properties [7]. The work in this paper uses compensated modulation with an improved arm voltage estimation technique which includes a closed loop control of the average energy [8].

III. Dynamic Equations

Before the dynamic equations can be presented, some basic definitions will be given. All equations are in per-unit with the base values given in the Appendix. The upper and lower arm voltages are decomposed into common mode, v_c, and differential components, v_s, as shown in (5).

$$v_c = \frac{1}{2}\left(v_u + v_l\right) \tag{5}$$

$$v_s = \left(-v_u + v_l\right) \tag{6}$$

The same decomposition can be applied to the upper and lower arm currents resulting in i_c and i_s as given by (7).

$$i_c = \frac{1}{2}\left(i_u + i_l\right) \tag{7}$$

$$i_s = \frac{3}{4}\left(i_u - i_l\right) \tag{8}$$

The differential components correspond to the ac side quantities. After applying this decomposition, the differential equation describing a simplified arm energy dynamics is given in Eq. (9).

$$\begin{aligned} \frac{\mathrm{d}}{\mathrm{d}t}w &= \frac{2}{c_p}\left[\frac{1}{2}v_{dc}^* i_c - \frac{1}{6}v_{sdq}^* \cdot i_{sd}\right] \\ &= \frac{1}{c_p}\left[v_{dc}^* i_c - \frac{1}{3}\left(v_{sd}^* i_{sd} + v_{sq}^* i_{sq}\right)\right] \end{aligned} \tag{9}$$

where w is the average arm energy, c_p is the per-unit arm equivalent capacitance, and i_c is the circulating current. v_{sdq}^* and i_{sdq} are the ac voltage reference and the ac current in dq domain, respectively. Eq. (9) shows that there will be a change in energy only when there is imbalance between the ac and dc side powers. The circulating current, i_c , plays a vital role in achieving power balance. Dynamics of i_c is captured by Eq. (10).

$$\frac{\mathrm{d}}{\mathrm{d}t}i_c = \frac{1}{l_{dc}}\Big(v_c^* - r_{dc} i_c\Big) \tag{10}$$

where l_{dc} and r_{dc} are the arm inductance and resistance in per-unit to the dc base values. The dc link voltage is governed by the differential equation given in Eq. (11).

$$\frac{\mathrm{d}}{\mathrm{d}t}v_{dc} = \frac{1}{c_{dc}}\Big(i_{dc} - 3i_c\Big) \tag{11}$$

where i_{dc} is the dc line current and c_{dc} is the equivalent dc side capacitance in per-unit. Finally, the ac current dynamics is given by Eq. (12) where ω is the fundamental frequency in rad/s and v_{gdq} is the grid voltage in dq domain. l_{ac} and r_{ac} are equivalent ac side inductance and resistance in per-unit.

$$\frac{\mathrm{d}}{\mathrm{d}t}i_{sdq} = \frac{1}{l_{ac}}\Big(v_{sdq}^* - v_{gdq} - r_{ac}\mathbf{I}\cdot i_{sdq} - \omega l_{ac}\mathbf{J}\cdot i_{sdq}\Big) \tag{12}$$

$$\mathbf{I} = \begin{bmatrix} 1 & 0 \\ 0 & 1 \end{bmatrix} \; and \; \mathbf{J} = \begin{bmatrix} 0 & -1 \\ 1 & 0 \end{bmatrix}$$

The sign conventions and additional variable definitions are shown in Fig. 1 The next section discusses the control structure used in this paper.

IV. Control Structure

Fig. 2 depicts block diagram of the controllers used in this paper. Only the control loops affecting active power are shown in the figure. Active power is controlled through the d-axis current, i_{sd}. Similarly, the average energy is controlled using the circulating current, i_c. The two control loops are coupled by the ac power. All the controllers in Fig. 2 are tuned using modulus and symmetric optimum techniques [9]. From Fig. 2, it can be observed that a change in ac power causes the energy to deviate. This triggers the energy controller to respond by adjusting i_c^* which in turn affects the dc power, P_{dc}. Therefore, deviations in ac power will eventually appear in the dc power. If the converter is providing POD, it has to inject oscillating power into the ac grid when the oscillation mode is excited. This oscillation will be exported to the dc side because of the action of the energy controller. Since the MMC is equipped with energy storage, it can provide the oscillating power from the capacitors keeping the dc side ideally unaffected. This is achieved by employing the auxiliary energy controller presented in the next section.

V. Proposed Auxiliary Energy Controller

The main function of the auxiliary controller is to inform the energy controller ($\mathbf{C_w}$ in Fig. 2) not to balance the oscillating part of the ac power (ΔP_{ac}) with the dc power. This is achieved by removing the contribution of ΔP_{ac} from the energy feedback signal (W_m). In such a way, $\mathbf{C_w}$ does not see the oscillation and hence will not export it to the dc side. Fig. 2 shows a functional block diagram of the auxiliary energy controller. The POD block is responsible for calculating the oscillating power (ΔP_{ac}^*) injected in to the ac grid when the electromechanical mode is excited. $\mathbf{H}_1$ and $\mathbf{H}_2$ are the equivalent transfer functions from P_{ac}^* to P_{ac} and from P_{ac} to W_m , respectively. The term equivalent is used to indicate that these transfer functions represent the gain and phase responses of the complete transfer functions at the oscillation frequency in the form of gain and lead-lag blocks. Such an implementation assumes that the system parameters are accurately known and there is only one mode of oscillation. These assumptions are made to simplify the initial implementation. If the parameters are not accurately known, the gains and phase angles can be tuned by performing tests before the converter is commissioned. The effect of parameter errors will be shown by simulation in Section VII. One important requirement for this control scheme to work is the availability of excess stored energy so that the POD does not disturb normal operation. This aspect will be discusses in the next section.

VI. Energy Storage Requirement

Calculation of the extra energy storage required to implement the proposed scheme will be presented in this section. First, derivation of the basic equations will be presented followed by potential options to obtain the required additional storage. Active power imbalance, Δp, and energy deviation, Δw, are related by (13).

$$\Delta w = \frac{2}{c_p} \int \Delta p \, \mathrm{d}t \tag{13}$$

which is obtained by integrating (9). Fig. 3 shows how the power injected by POD typically looks. The resulting energy deviation, as given by (13), is the area under the curve. It is assumed that the oscillation mode, on which the POD is applied, is stable. This implies that the area under subsequent half-cycles diminishes with time. Therefore, the worst case energy deviation is caused by the first swing which is indicated by the gray area in Fig. 3. The maximum energy deviation, Δw_{max}, can be computed using (14).

$$\Delta w_{max} = \frac{2}{c_p} \frac{2\hat{p}}{\omega_{osc}} \tag{14}$$

where $\hat{p}$ is peak value of the oscillation. Eq. (14) over-estimates the deviation since it ignores the effect of damping. This is justified because the damping is not constant and the intention is to consider the worst possible case which is when the damping is 0. The corresponding deviation in arm voltage, Δv_{max}, can be computed, from the fact that $w = v^2$, using (15).

$$\Delta w_{max} = \Delta v_{max} \left(\Delta v_{max} + 2v \right) \tag{15}$$

where v is the nominal arm voltage. Having defined the maximum voltage deviation, the requirement for the extra energy storage can now be defined. The main constraint is that the arm voltages have to be more than the ac peak voltage (assuming sinusoidal modulation) in order to avoid over-modulation. Δv can be positive or negative depending on the sign of POD power injection. When Δv is negative, there is a risk of over-modulation. A positive Δv, on the other hand, can result in over-voltage in the SMs. Therefore, the arm voltage should satisfy the constraint in (16).

$$\hat{v}_{ac} + \Delta v_{max} \leq v \leq V_{rated} - \Delta v_{max} \tag{16}$$

where $\hat{v}_{ac}$ is the maximum ac peak voltage in pu and V_{rated} is the sum of rated voltages of the SMs. From (16), it can be seen that the arm voltage has to be greater than $1.0\ pu$, since $\hat{v}_{ac}$ is typically close to $1.0\ pu$, in order to provide the proposed service. This can be achieved by increasing either the number of SMs, N, or the SM voltage, V_{SM}. The relation between these quantities and the stored energy, W in joules, is given in (17).

$$W = \frac{1}{2} \frac{C_{SM}}{N} \left(N \cdot V_{SM} \right)^2 \tag{17}$$

where C_{SM} is the Sub-Module capacitance. Increasing C_{SM} is not considered because it only helps in reducing Δv_{max} but not to increase v. The two options will be discussed in the following sections.

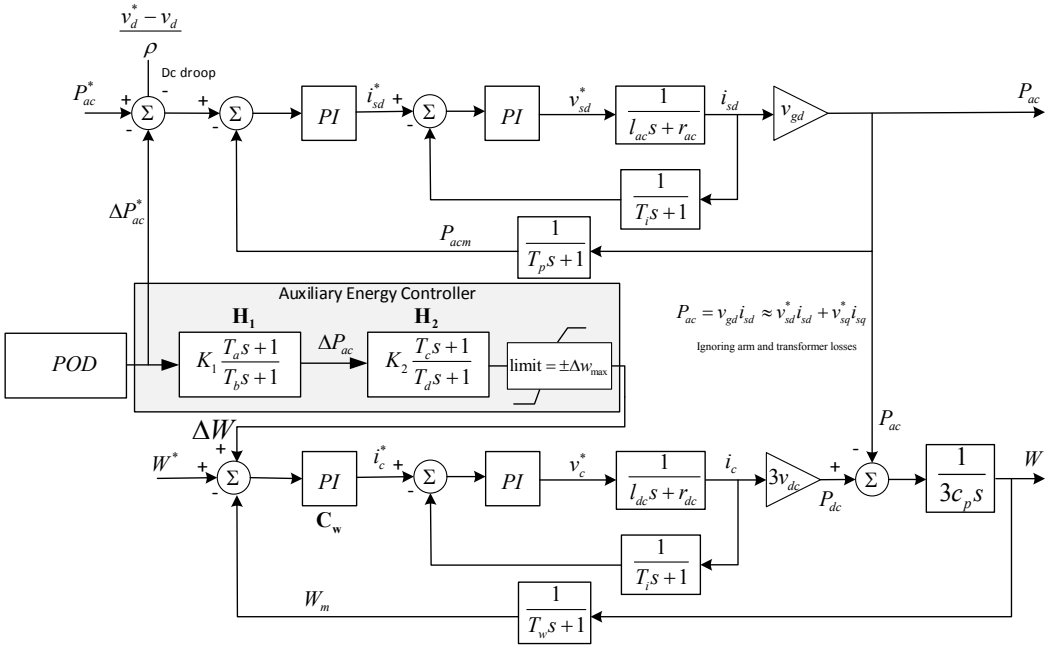

Fig. 2. Auxiliary controller block diagram.

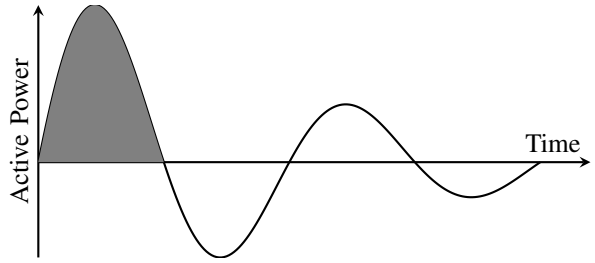

Fig. 3. Active power oscillation.

TABLE I
HVDC CONVERTER PARAMETERS[10]

Parameter	Value
Base apparent power, S_b	900 MVA
Base dc voltage, V_b^{dc}	640 kV
Frequency, ω	$2\pi 50$ rad/s
Arm capacitance, $C_{arm} = C_{SM}/N$	29 μF
Arm inductance, L_{arm}	84 mH
Arm resistance, R_{arm}	0.885 Ω
Transformer reactance, X_t	17.7 Ω
Transformer resistance, R_t	1.77 Ω

A. Increasing the Number of Sub-Modules

The effect of introducing additional SMs will be investigated by replacing N by $(1+\alpha)\,N$ in (17). Where α is a number between 0 and 1. The additional energy due to α, ΔW^{α}, is given by (18).

$$\Delta W^{\alpha} = \alpha W \tag{18}$$

where W is the nominal energy calculated using (17). The maximum available POD power can be calculated by combining (18) with (14) as shown in (19).

$$\hat{P}_{max} = \frac{1}{2}\Delta W_{max} \cdot \omega_{osc} \cdot \alpha \times 6 \; [MW] \tag{19}$$

where $\Delta W_{max} = W_b \cdot \Delta w_{max}$ is the maximum energy deviation in joules. The factor 6 is included because the ac power oscillation is assumed to be shared equally by the 6 arms. $\hat{P}_{max}$ is calculated for combinations of ω_{osc} and α using the parameters in Table I. The result is shown in Fig. 4. It can be seen that the maximum available POD power is very limited at low frequencies. The amount of extra storage gained is linearly proportional to α. This option can be more attractive because there will usually be some extra modules added for redundancy. These modules can be utilized for the POD service.

B. Increasing the Rated Voltage of Sub-Modules

In this section an increase in SM voltage from V_{SM} to $(1+\beta)V_{SM}$ is considered. Where β is a number between 0 and 1. By following a similar approach to the previous section, the maximum POD power can be calculated as shown in (20). A plot of $\hat{P}_{max}$ for different values of β is depicted in Fig. 5.

$$\hat{P}_{max} = \frac{1}{2}\Delta W_{max} \cdot \omega_{osc} \cdot \left(\beta^2 + 2\beta\right) \times 6 \; [MW] \tag{20}$$

It can be observed that more POD power can be obtained by increasing β compared to α. However, this option will likely be more expensive since it requires upgrade of all SMs. The optimal solution, which is a combination of the two options, is a result of an optimization problem which is beyond the scope of this paper. A value of $\beta = 0.15$ which is equivalent to $\alpha = 0.32$ is assumed for simulation in the next section. It should be noted that the maximum POD power discussed

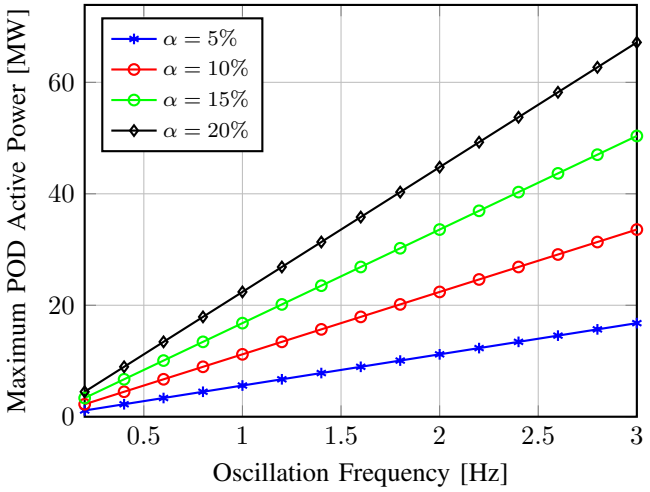

Fig. 4. Maximum POD power as a function of oscillation frequency for different values of α.

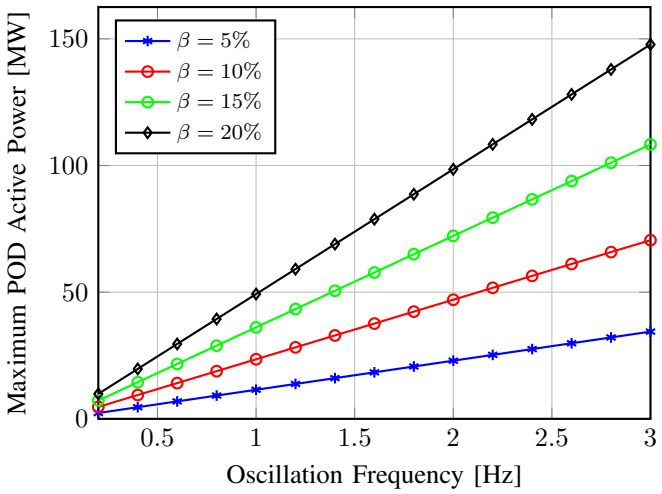

Fig. 5. Maximum POD power as a function of oscillation frequency for different values of β.

in this section is the maximum that can be provided without disturbing the dc side. The converter can still provide more POD power at the cost dc side oscillation. In such cases, output of the Auxiliary controller should be limited to Δw_{max} defined in this section. Two options for limiting the output will be compared by simulation in the next section.

VII. Simulation Results

Simulation results showing effectiveness of the proposed auxiliary controller are presented in this section. The simulation model is based on the four terminal test grid proposed in [10], (Fig. 6). The model is implemented in SIMULINK with the parameters shown in Table I. Effect of the POD block is emulated by injecting oscillating power of magnitude $0.06\ pu$ and damping of $\zeta \approx 5\%$ at $t = 7\ sec$ in to that ac grid connected to Converter 3, (Fig. 6). Each terminal is droop controlled with a voltage droop of 5%. The cables are modeled

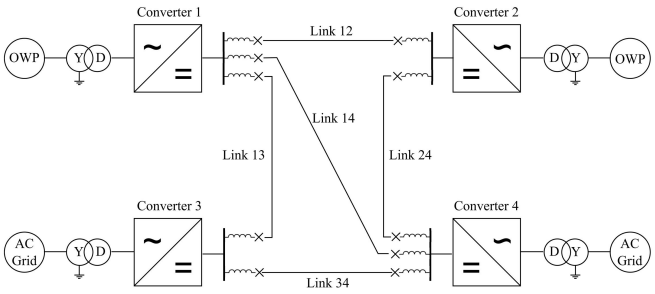

Fig. 6. Test grid used for simulation [10]

TABLE II
Simulation Test Cases

Case No.	Description
Case 1	Base case: No POD action
Case 2	POD action without Aux. Controller
Case 3	POD action + Aux. Controller
Case 4	POD with different frequencies: 1 Hz, 2 Hz, and 5 Hz.
Case 5	Effect of output limiter
Case 6	Effect of parameter inaccuracies

using the frequency dependent model proposed in [11]. All converters are MMCs which are modeled using average arm capacitor dynamics [12]. Six test cases described in Table II will be used to test the proposed scheme.

The results are displayed in Figs. 7 to 13. From the base case (Fig. 7), it can be seen that the system exhibits a stable operation under normal conditions. All the reference signals are rate-limited by using first order low pass filters. The difference between the ac and dc powers in Fig. 7b is because of losses in the converter. With the emulated POD power injected from converter 3 (Fig. 8), the dc voltages exhibit oscillations as shown in Fig. 9a. When the auxiliary controller is enabled, the POD power is diverted into the arm capacitors instead of the dc side as is evident from Fig. 8b. Doing so, the controller can effectively remove the oscillation from the dc side, (Fig. 9b).

Because of the power taken from the capacitors, the average stored energy exhibits oscillatory response, (Fig. 10a). This confirms that the oscillation is supplied from the arm capacitors instead of the dc side. The worst case deviation in energy is computed using (14) to be ≈ 0.25 while the value read from Fig. 10a is ≈ 0.15. The difference is because the effect of damping which was neglected in (14). Fig. 10b shows impact of the POD action on the stored energy of converter 2 where it is clearly visible that the converter does not see the oscillation when the proposed controller is active. In order to investigate the correlation between energy deviation and oscillation frequency, POD at different frequencies was also simulated. Fig. 11a shows stored energy of the POD terminal with the auxiliary controller enabled. It can be clearly seen that the deviation grows with decrease in frequency. This is in-line with the discussion in Section VI and (14). The corresponding power injections are depicted in Fig. 11b where it can be

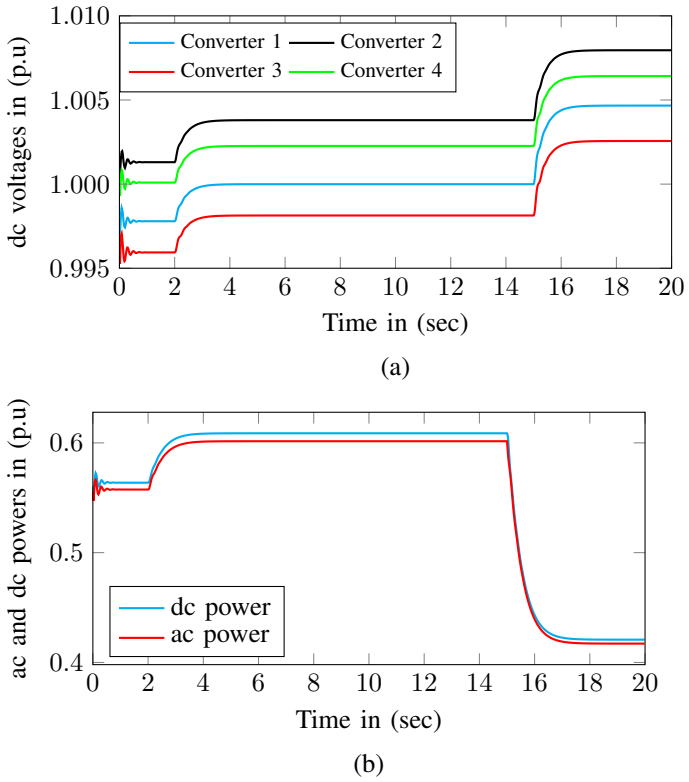

Fig. 7. Base case (Case 1) system performance: (a) dc voltages and (b) ac and dc powers of converter 1

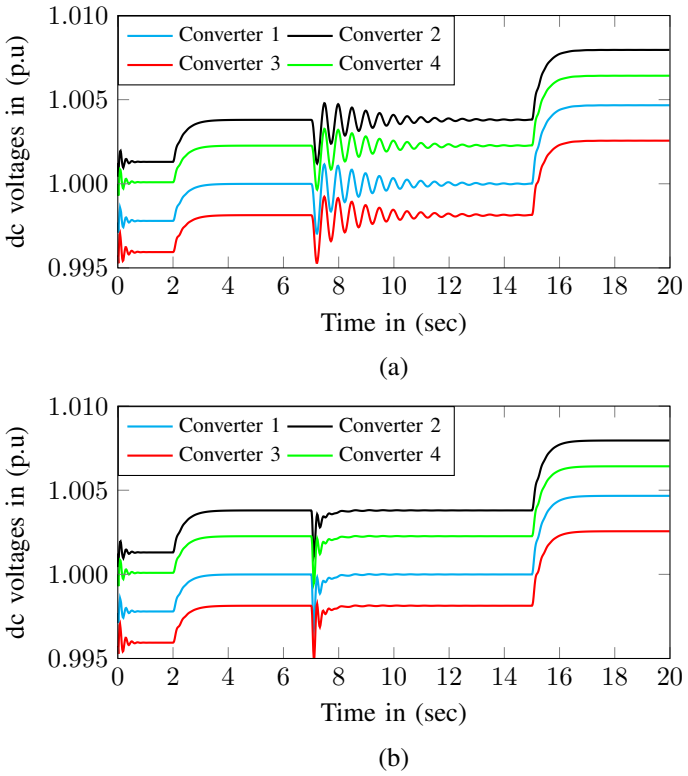

Fig. 9. dc voltages with POD: (a) Case 2–without Aux control and (b) Case 3–with Aux control

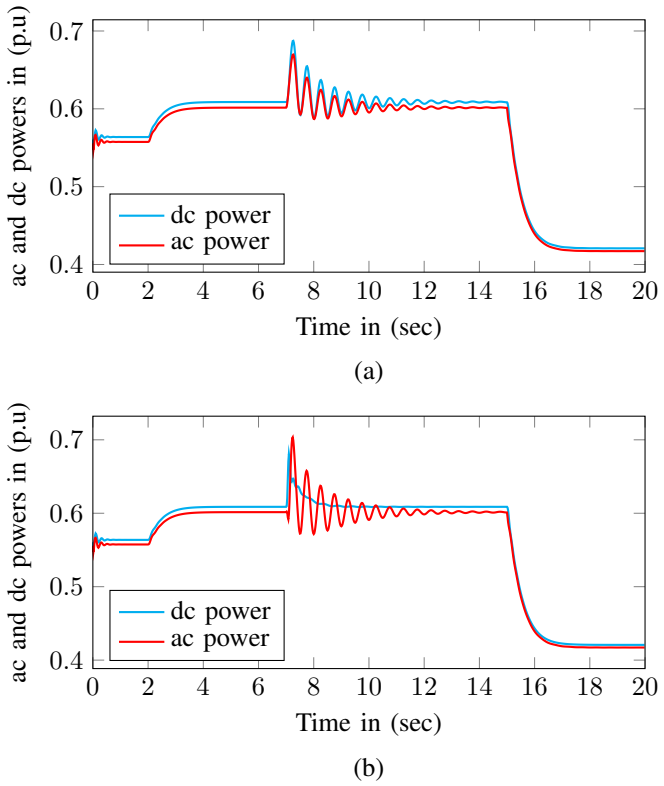

Fig. 8. ac and dc powers of converter 1 with POD: (a) Case 2–without Aux control and (b) Case 3–with Aux control

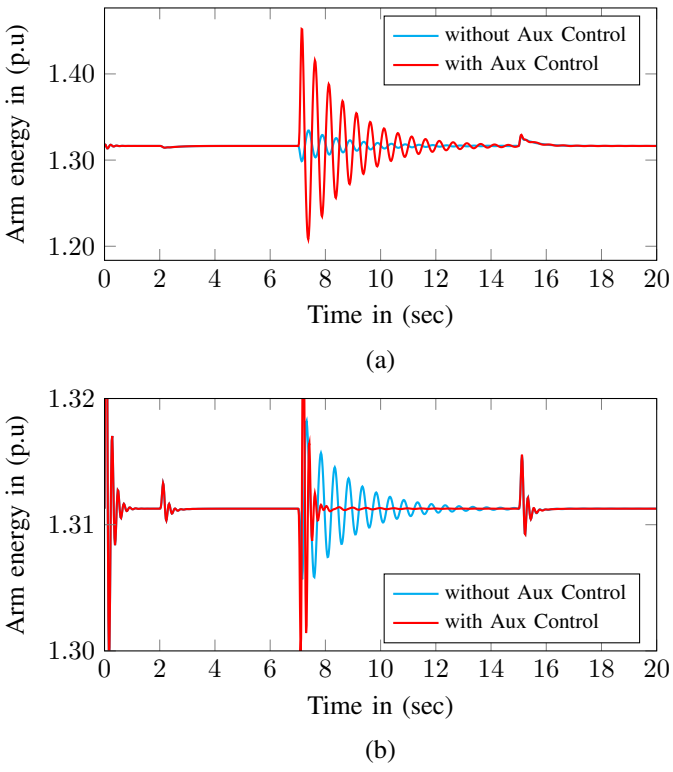

Fig. 10. Arm energies with (Case 2) and without (Case 3) Aux control: (a) Converter 3 and (b) Converter 2

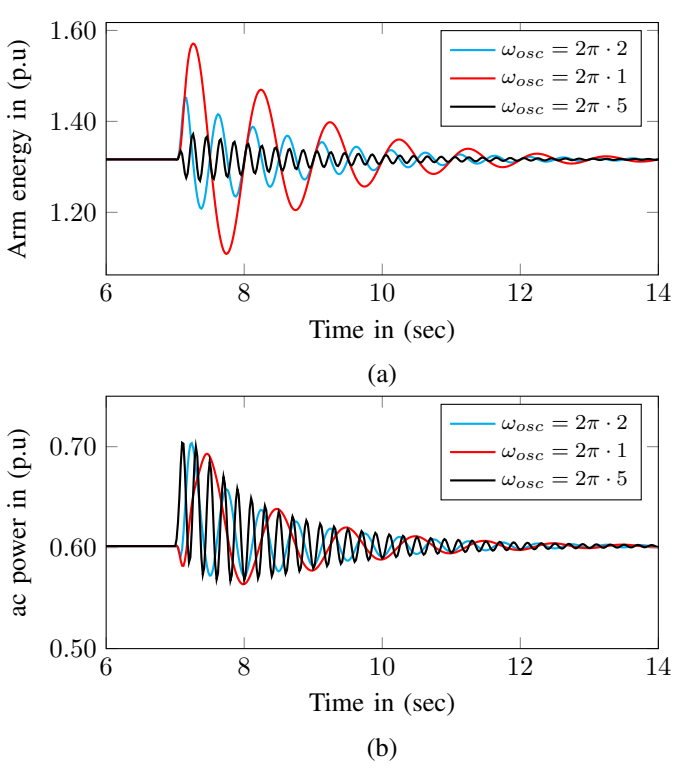

Fig. 11. Results at different oscillation frequencies with Aux control: (a) Arm voltages and (b) ac power at converter 3.

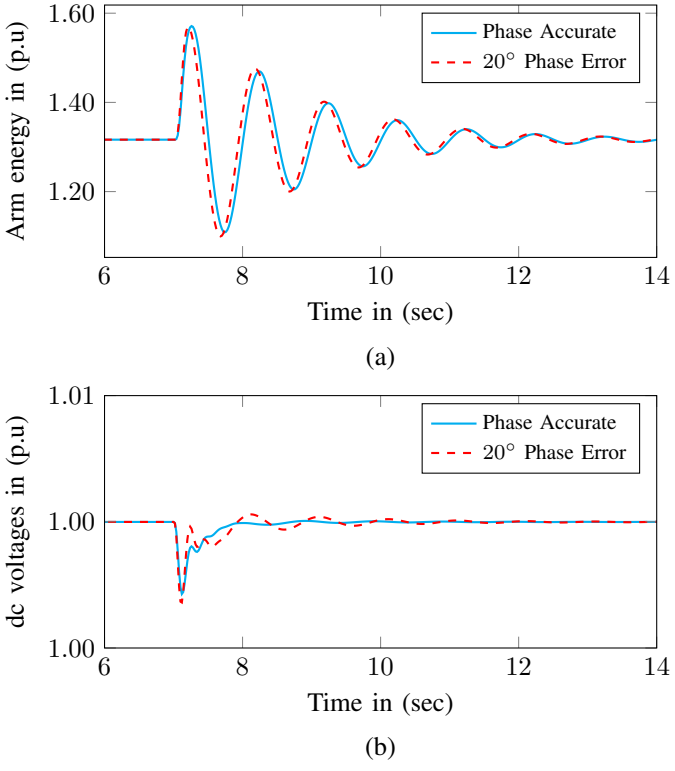

Fig. 13. Effect of phase angle error (Case 4, $\omega_{osc} = 2\pi \cdot 1$): (a) Arm voltages and (b) dc voltages.

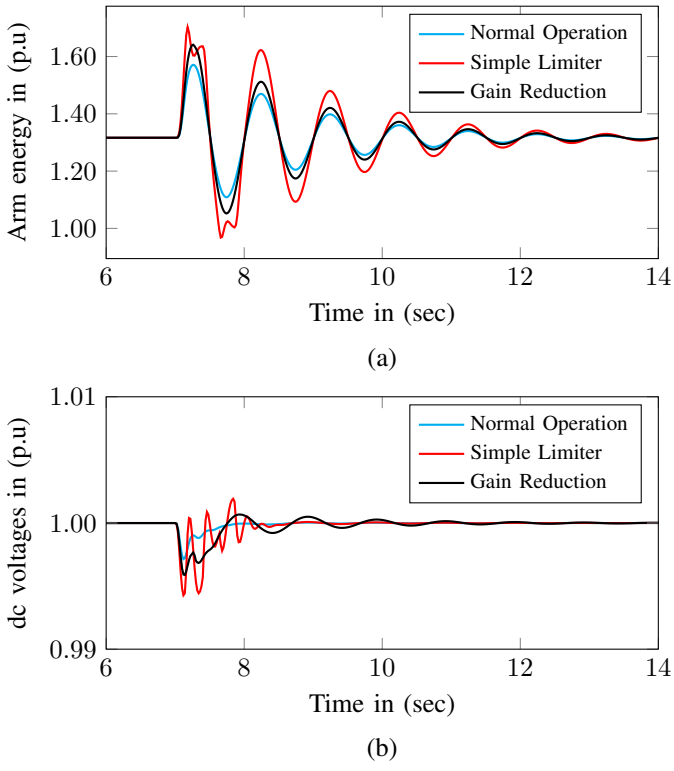

Fig. 12. Effect of output limiter on the Aux. controller (Case 4 $\omega_{osc} = 2\pi \cdot 1$): (a) Arm voltages and (b) dc voltages

seen that the magnitudes are the same in all the cases. The auxiliary controller block output is limited to $\approx \pm 0.32$ pu which is equivalent to ± 0.15 pu limit on the arm voltage. They are chosen to keep the arm energy above 1.0 pu in all cases. Fig. 12 shows how the system responds when the energy deviation is larger than the limits. It can be seen that the simple limiter (which is a simple clamping limiter) is able to keep the energy deviation within the specified limits. However, the dc voltage (Fig. 12b) exhibits a larger magnitude distortion during the period when the output is limited. The second option to limit the output is to reduce gain of the auxiliary controller which in effect reduces the amount of power diverted into the capacitors. This results in a smoother limit but at the cost of more oscillation in the dc voltage, (Fig. 12b). Combining the two approaches, dynamic adjustment of the gain with simple limiter on the output can give better results. Finally, the effect of parameter inaccuracies is studied. Parameter errors result in either gain or phase error in the oscillation. Effect of phase angle error is depicted in Fig. 13. The effect of gain error is similar to the gain reduction case in Fig. 12. The main consequence is that some of the oscillating power is taken from the dc side resulting in dc voltage oscillation, Fig. 13b. This implies that scheme can work well even with significant parameters errors. Further improvement can be gained by tuning the parameters from test results.

VIII. Conclusion

This paper proposes a control scheme to minimize the impact of POD action on the dc side of an MMC converter station. This is achieved by diverting the oscillating component of the ac power into the arm capacitors. Simulation results show that the scheme is promising. The benefits come at the cost of increased energy storage requirement. The extra energy storage requirement and potential options to achieve this have been discussed in this paper. Increasing the number of modules or the rated voltage of each module can be used to get the extra storage. A combination of the two should be used to get optimal solution. It was found that the amount of required storage increases at low frequencies. In cases when enough storage is not available, partial cancellation of the oscillation can be done with the help of output limiters. Output limits play a vital role in the performance of the scheme. Simple limiter and gain reduction were evaluated. Dynamic gain adjustment can give better results. The scheme can also be extended to support multiple oscillation frequencies.

Appendix

The base values used for per-unit calculations are depicted in (21).

$$
\begin{aligned}
I_b^{ac} &= \frac{2S_b}{3V_b^{ac}} \quad Z_b^{ac} = \frac{V_b^{ac}}{I_b^{ac}} \quad I_b^{dc} = \frac{S_b}{V_b^{dc}} \quad Z_b^{dc} = \frac{V_b^{dc}}{I_b^{dc}} \\
L_b^{ac} &= Z_b^{ac} \quad C_b^{ac} = \frac{1}{Z_b^{ac}} \quad L_b^{dc} = Z_b^{dc} \quad C_b^{dc} = \frac{1}{Z_b^{dc}} \\
V_b^{dc} &= 2V_b^{ac} \quad W_b = \frac{C_b^{dc}\left(V_b^{dc}\right)^2}{2}
\end{aligned} \tag{21}
$$

References

[1] L. Harnefors, N. Johansson, L. Zhang, and B. Berggren, "Interarea oscillation damping using active-power modulation of multiterminal HVDC transmissions," *IEEE Trans. Power Syst.*, vol. 29, no. 5, pp. 2529–2538, 2014.

[2] L. Zeni, R. Eriksson, S. Goumalatsos, M. Altin, P. Sørensen, A. Hansen, P. Kjær, and B. Hesselbæk, "Power Oscillation Damping From VSC HVDC Connected Offshore Wind Power Plants," *IEEE Trans. Power Deliv.*, vol. 31, no. 2, pp. 829–838, Apr. 2016.

[3] M. Ndreko, A. van der Meer, M. Gibescu, B. Rawn, and M. van der Meijden, "Damping Power System Oscillations by VSC-Based HVDC Networks: A North Sea Grid Case Study," in *Proc. WIW 2013: 12th Int. Workshop Large-Scale Integration of Wind Power Into Power Systems as Well as on Transmission Networks for Offshore Wind Power Plants*, 2013.

[4] N. T. Trinh, I. Erlich, and S. P. Teeuwsen, "Methods for utilization of MMC-VSC- HVDC for power oscillation damping," in *2014 IEEE PES General Meeting — Conference Exposition*, Jul. 2014, pp. 1–5.

[5] G. Bergna Diaz, J. A. Suul, and S. D'Arco, "Small-signal state-space modeling of modular multilevel converters for system stability analysis," in *Energy Conversion Congress and Exposition (ECCE), 2015 IEEE*. IEEE, 2015, pp. 5822–5829.

[6] L. Ängquist, A. Haider, H. P. Nee, and H. Jiang, "Open-loop approach to control a Modular Multilevel Frequency Converter," in *Proc. 2011-14th European Conf. Power Electronics and Applications (EPE 2011)*, Aug. 2011, pp. 1–10.

[7] A. Antonopoulos, L. Ängquist, L. Harnefors, K. Ilves, and H. P. Nee, "Global Asymptotic Stability of Modular Multilevel Converters," *IEEE Trans. Ind. Electron.*, vol. 61, no. 2, pp. 603–612, Feb. 2014.

[8] A. A. Taffese, E. Tedeschi, and E. de Jong, "Arm Voltage Estimation Method for Compensated Modulation of Modular Multilevel Converters," in *12th IEEE PES PowerTech Conference*, Manchester, UK, Jun. 2017.

[9] J. W. Umland and M. Safiuddin, "Magnitude and symmetric optimum criterion for the design of linear control systems: What is it and how does it compare with the others?" *IEEE Trans. Ind. Appl.*, vol. 26, no. 3, pp. 489–497, May 1990.

[10] W. Leterme, N. Ahmed, J. Beerten, L. Angquist, D. V. Hertem, and S. Norrga, "A new HVDC grid test system for HVDC grid dynamics and protection studies in EMT-type software," in *11th IET International Conference on AC and DC Power Transmission*, Feb. 2015, pp. 1–7.

[11] J. Beerten, S. D'Arco, and J. A. Suul, "Frequency-dependent cable modelling for small-signal stability analysis of VSC-HVDC systems," *Transm. Distrib. IET Gener.*, vol. 10, no. 6, pp. 1370–1381, 2016.

[12] L. Harnefors, A. Antonopoulos, S. Norrga, L. Angquist, and H. P. Nee, "Dynamic Analysis of Modular Multilevel Converters," *IEEE Trans. Ind. Electron.*, vol. 60, no. 7, pp. 2526–2537, Jul. 2013.